Research Paper
Computational Methods for Differential Equations
http://cmde.tabrizu.ac.ir
Vol. *, No. *, *, pp. 1-22
DOI:10.22034/cmde.2026.70096.3465

Numerical methods for the fractional generalized Korteweg–de Vries–Burgers equation with the Caputo–Prabhakar derivative using GRBF and RBF–FD approaches

Safar Irandoust-pakchin*, **MohammadHossein Derakhshan, and Somaiyeh Abdi Mazraeh**
Department of Applied Mathematics, Faculty of Mathematics, Statistics and Computer Sciences,University of Tabriz, Tabriz, Iran.

Abstract

This work is devoted to the numerical treatment of the generalized Korteweg–de Vries–Burgers (GKdVB) equation involving a time–fractional derivative defined in the sense of the regularized Caputo–Prabhakar operator. To approximate the solution of this fractional nonlinear model, two meshless computational frameworks are employed. The first approach is the global radial basis function (GRBF) method, which utilizes globally supported basis functions to obtain highly accurate spatial approximations. The second approach is the radial basis function finite difference (RBF–FD) scheme, where the flexibility of radial basis functions is combined with the computational efficiency of finite difference–type discretizations. These two strategies provide complementary advantages, balancing accuracy, computational efficiency, and adaptability to complex domains. A stability analysis of the resulting schemes is also presented to assess the reliability of the numerical approximations. To illustrate the performance of the proposed techniques, a representative numerical experiment is carried out, and the obtained results are reported through graphical and tabulated data. The numerical findings confirm that the GRBF and RBF–FD approaches provide accurate and stable approximations for the fractional GKdVB equation and demonstrate their potential for applications in various scientific and engineering problems involving nonlinear fractional models.

Keywords. Generalized Korteweg–de Vries–Burgers, Global radial basis function, Radial basis function finite difference, Regularized Caputo–Prabhakar operator, Stability.

2010 Mathematics Subject Classification. 35R11; 65M70; 65N35.

1. Introduction

The study of partial differential equations (PDEs) involving fractional operators has become increasingly important in both physics and applied mathematics [8, 24–26, 30]. These equations play a crucial role in modeling and understanding complex systems whose behavior cannot be adequately described by classical integer-order derivatives. In many real-world phenomena, such as anomalous diffusion, viscoelasticity, signal processing, and fluid dynamics, the underlying processes exhibit memory effects and spatial non-locality. Fractional derivatives naturally capture these features due to their non-local definition, which incorporates the influence of past states and extended spatial interactions. Consequently, fractional PDEs provide a more accurate and flexible framework for describing physical behaviors that go beyond the scope of traditional models.

The Mittag–Leffler (ML) function, named after the Swedish mathematician Magnus Gustaf Mittag–Leffler, was introduced in the early 1900s during his investigations into techniques for summing divergent series. Since its introduction, numerous generalizations of this function have been developed and extensively studied, with entire monographs dedicated to exploring its properties and applications. In the field of fractional calculus, the ML function plays a role comparable to that of the exponential function in the theory of ordinary calculus. Specifically, it provides the natural framework for describing solutions to many problems involving derivatives of non-integer order, making it a cornerstone of modern fractional analysis. In the last few decades, a three-parameter generalization of the Mittag–Leffler function, commonly referred to as the Prabhakar function, has gained significant attention. This extension introduces

Received: 07 November 2025; Accepted: 04 July 2026.
∗ Corresponding authors. Emails: s.irandoust@tabrizu.ac.ir.

TABLE 1. Special cases of the GKdVB model.

Case	Coefficient Conditions	Equation Name
1	$\eta = 0,\ \varrho = 0,\ \xi \neq 0$	KdV equation
2	$\xi = 0,\ \varrho = 0,\ \eta \neq 0$	Modified KdV equation
3	$\varrho = 0,\ \xi \neq 0,\ \eta \neq 0$	Combined KdV equation
4	$\eta = 0,\ \sigma = 0,\ \xi \neq 0,\ \varrho \neq 0$	KdV–Burgers equation

additional flexibility compared to the classical ML function, making it a powerful tool in modeling complex processes that exhibit memory effects and anomalous dynamics. A large part of the current interest in the Prabhakar function arises from its effectiveness in modeling relaxation and dielectric response phenomena of the Havriliak–Negami type. This model of complex susceptibility was originally proposed to capture both nonlocal memory effects and nonlinear behavior observed in disordered and heterogeneous materials [34]. Beyond dielectric physics, the Prabhakar function has found relevance in a broad spectrum of disciplines: it appears in probability theory [21], the analysis of stochastic processes [12], systems exhibiting anisotropic properties [10], and in the field of fractional viscoelasticity [20]. It also plays an important role in solving fractional boundary–value problems [9, 21], in dynamical models of stellar systems [7], and in formulations involving fractional and integral differential equations [4]. In particular, the temporal evolution of polarization in Havriliak–Negami models, as well as the processes mentioned above, can be rigorously described through integral and differential operators built upon the Prabhakar kernel [11, 12].

In this study, we investigate approximate solutions of the generalized Korteweg–de Vries–Burgers (GKdVB) model incorporating the regularized Caputo–Prabhakar derivative. The model is presented as follows:

$$ {}^{C}\mathcal{D}^{\nu}_{\alpha,\beta,\mu} w(x,t) + (\xi + \eta w)\, w\, \frac{\partial w(x,t)}{\partial x} + \varrho \frac{\partial^2 w(x,t)}{\partial x^2} + \sigma \frac{\partial^3 w(x,t)}{\partial x^3} = 0, \quad x \in (a,b), \quad t \in (0,T],\ \beta \in (0,1), \tag{1.1} $$

under the following initial and boundary conditions:

$$ w(x,0) = s(x), \quad a \leq x \leq b, \tag{1.2} $$

$$ w(a,t) = f_1(t), \quad w(b,t) = f_2(t), \quad t \geq 0. \tag{1.3} $$

In Eq. (1.1), the parameters $\xi, \eta, , \varrho, \sigma, a, b, s(x), f_1(t), f_2(t)$ are all known, $\varrho \leq 0$ representing dissipative effects and σ modeling dispersion. Table 1 summarizes several well-known nonlinear evolution equations that can be obtained as particular cases of the generalized Korteweg–de Vries–Burgers (GKdVB) model through suitable choices of the coefficients. By adjusting the parameters ξ, η, ϱ, and σ, the proposed formulation is capable of representing different physical regimes that arise in nonlinear wave propagation, dispersive media, and dissipative systems. In particular, when the quadratic nonlinear contribution vanishes ($\eta = 0$) and the dissipative term is neglected ($\varrho = 0$), Eq. (1.1) reduces to the classical Korteweg–de Vries (KdV) equation, which describes the propagation of solitary waves in weakly dispersive media. If the linear nonlinear coefficient is removed ($\xi = 0$) while the cubic nonlinear term remains ($\eta \neq 0$) and $\varrho = 0$, the model leads to the modified Korteweg–de Vries (mKdV) equation, which arises in several nonlinear physical contexts such as plasma physics and fluid dynamics. When both nonlinear terms are present ($\xi \neq 0$ and $\eta \neq 0$) and the dissipative effect is absent ($\varrho = 0$), the equation reduces to the combined KdV equation, capturing the interaction between quadratic and cubic nonlinearities. Finally, by eliminating the dispersive term ($\sigma = 0$) and retaining the dissipative contribution ($\varrho \neq 0$) together with the quadratic nonlinearity ($\eta = 0$), the GKdVB equation simplifies to the well-known KdV–Burgers equation, which models the combined effects of nonlinearity, dissipation, and wave propagation. These reductions highlight the generality and flexibility of the GKdVB model, demonstrating that it provides a unified mathematical framework capable of encompassing several important nonlinear wave equations as special cases. The symbol ${}^{C}\mathcal{D}^{\nu}_{\alpha,\beta,\mu}$ in Equation (1.1) represents the regularized Caputo–Prabhakar derivative [21], which will be explained in more detail in the next section.

This paper is devoted to the investigation of numerical techniques for solving the generalized Korteweg–de Vries–Burgers (GKdVB) equation that incorporates the generalized fractional derivative, known as the regularized Caputo–Prabhakar derivative. This type of fractional operator provides a more flexible framework for modeling memory and hereditary

effects in complex physical systems. To approximate the solution of the fractional GKdVB model, two distinct meshless numerical strategies are employed. The first approach relies on the global radial basis function (GRBF) method, which makes use of globally supported basis functions to provide accurate approximations. The second approach is the radial basis function finite difference (RBF-FD) scheme, which combines the flexibility of meshless methods with the efficiency of finite difference techniques, making it suitable for handling problems defined on irregular or higher-dimensional domains. The paper also presents a detailed stability analysis of these methods to ensure the reliability of the computed solutions. Furthermore, a comprehensive numerical experiment is carried out, where the effectiveness of the proposed algorithms is tested. The results are displayed in both graphical and tabular formats, highlighting the accuracy, efficiency, and robustness of the techniques. These demonstrations confirm the potential of GRBF and RBF-FD methods as powerful tools for solving fractional partial differential equations of the GKdVB type.

Finding exact analytical solutions for partial differential equations that involve fractional operators is often a very challenging task. In many cases, such solutions cannot be obtained using traditional analytical techniques. Because of this difficulty, researchers rely on numerical methods, which make it possible to approximate the true solution with a high degree of accuracy. These methods are designed to minimize errors so that the difference between the exact and approximate solutions remains very small. Numerical approaches are especially important in studying complex physical processes where fractional models are used, such as heat conduction with memory effects, anomalous diffusion, or viscoelastic behavior. By applying these techniques, we can better understand the dynamics of such systems and gain insights that would otherwise be inaccessible. In this work, we present and discuss some of the main numerical strategies commonly employed for solving fractional models and highlight their effectiveness in capturing the essential features of these phenomena. Franke and Schaback [19] explored meshfree collocation techniques using radial basis functions to estimate smooth solutions for systems involving linear differential or integral operators. Unlike conventional strategies that primarily target elliptic problems, these meshfree methods are versatile and can be applied to a wide array of differential and integral equations. Salehi [39] introduced a meshfree collocation approach to tackle the two-dimensional multi-term time fractional diffusion-wave equation. In this method, the spatial approximation is built using shape functions derived from the moving least squares reproducing kernel particle technique. Mohebbi et al. [33] developed a numerical technique to solve the time-fractional nonlinear Schrödinger equation in both one- and two-dimensional settings, commonly encountered in quantum mechanics. This meshless approach has demonstrated effectiveness not only in traditional quantum mechanical problems but also across a range of engineering and physical applications. Fedoseyev et al. [18] investigated the multiquadric (MQ) radial basis function approach, a modern meshless collocation technique using global basis functions. Initially, the MQ method was applied for interpolating scattered data and was found to achieve exponential convergence in such interpolation tasks. Radmanesh and Ebadi [37] examined the local radial basis function (LRBF) method, which is highly effective for solving variable-order time-fractional evolution equations. Compared to the traditional global RBF collocation (GRBFC) method, it significantly lowers computational costs. In this study, an efficient meshless LRBF collocation technique is proposed to solve two-dimensional (2D) fractional evolution equations of arbitrary fractional order, even in domains with complex shapes. Qiao et al. [36] introduced a meshless local radial point collocation technique for numerically solving time-fractional convection-diffusion equations on closed surfaces in $\mathbb{R}^3$. They applied the second-order shifted Grünwald scheme for time discretization, and all calculations were performed using extrinsic coordinates to avoid distortions and singularities. Abbaszadeh et al. [5] explored a local meshless collocation method for the two-dimensional Klein-Kramers equation with a fractional time derivative in the Riemann–Liouville sense. This equation models sub-diffusion under the influence of an external force field in phase space. Mirzaee and Samadyar [32] proposed a semi-discrete numerical approach to solve time–fractional stochastic advection–diffusion equations. This method combines a finite difference scheme with radial basis function (RBF) interpolation to transform the problem into a linear system of algebraic equations. Essentially, the time-fractional stochastic advection–diffusion equation is first converted into elliptic stochastic differential equations using the finite difference method. Haghi and Ilati [23] developed a high–order local meshless technique for solving the two-dimensional distributed–order time-fractional cable equation on both regular and irregular domains. They approximate the distributed-order integral using the Gauss–Legendre quadrature formula and then apply a second–order weighted and shifted Grünwald difference (WSGD) scheme for the Riemann-Liouville time

derivatives. The stability and convergence of the time-discrete scheme are analyzed using the energy method. Aslefallah and Shivanian [6] presented a numerical approach for solving the nonlinear time-fractional integro-differential reaction–diffusion equation involving the Caputo fractional derivative. Their method eliminates the spatial variable using the finite difference Θ–method, ensuring stability of the solution. Soleymani and Zhu [41] investigated a Hermite finite difference scheme based on radial basis functions with a Gaussian kernel applied on graded meshes. Their theoretical analysis demonstrates higher convergence rates for approximating derivatives of functions. Li [31] presented a method using radial basis functions (radial powers) to approximate derivatives from one-dimensional scattered noisy data. This approach is also applicable to estimating Caputo fractional derivatives of order between 0 and 1. Wei et al. [42] explored and extended the local radial basis function (RBF) method for solving two-dimensional variable–order time-fractional diffusion equations in domains with complex shapes. Goufo [22] investigated extending the analysis of the Korteweg–de Vries–Burgers equation with two perturbation levels to fractional differentiation without singularities. The study uses the Caputo–Fabrizio fractional derivative, which features a nonsingular kernel, to formulate the model. Rida and Hussien [38] proposed a collocation method based on double summations of Mittag–Leffler functions to solve fractional-order Korteweg–de Vries (KdV) and Burgers equations with given initial and boundary conditions. Yu et al. [43] developed a space–time Petrov–Galerkin method for third- and fifth–order time–fractional Korteweg–de Vries–Burgers equations. Their approach employs Legendre and Jacobi polynomials, with the fractional component's basis functions constructed using generalized Jacobi functions that account for the weak solution singularities. Singh et al. [40] presented a numerical method to approximate the Caputo-Prabhakar derivative and applied it to solve the time-fractional advection-diffusion equation in the Caputo-Prabhakar sense, which is commonly used in fluid dynamics. Derakhshan and Aminataei [17] proposed a new numerical approach based on the Adams-Bashforth method for solving two-component time-fractional differential equations involving the Caputo-Prabhakar derivative of order μ. They also discussed the existence and uniqueness of solutions for these two-component equations using this method. In recent years, fractional differential equations have attracted significant attention due to their capability to model memory and hereditary properties in complex physical and engineering systems. A wide range of analytical and numerical techniques has been developed to handle time–space fractional models, distributed-order operators, and stochastic fractional systems. One important class of problems involves fractional wave and diffusion equations with distributed-order operators. Kosari and Derakhshan [29] proposed an efficient numerical approach for solving a time–space fractional wave model of multiterm order involving Riesz fractional operators of distributed order with weakly singular kernels, accompanied by a detailed stability analysis. In a related direction, Park et al. [35] developed a fourth-order accurate numerical scheme for distributed-order Riesz space fractional diffusion equations incorporating the time-fractional regularized Caputo–Prabhakar derivative, demonstrating high accuracy and robustness. Hybrid and high-accuracy numerical approaches for time–space fractional diffusion models have also been explored. Derakhshan et al. [15] introduced a hybrid numerical method for solving diffusion equations involving Caputo and Riesz fractional derivatives, achieving improved convergence behavior. Furthermore, Derakhshan [16] investigated the stability and convergence of a meshless Newmark scheme for nonlinear distributed-order Caputo models on complex domains, providing rigorous theoretical justification along with computational validation. The stability analysis of fractional systems remains a fundamental topic. Derakhshan et al. [14] studied the asymptotic stability of Weber fractional differential systems, offering theoretical insights into long-term dynamical behavior. Chen et al. [13] analyzed the stability of the time-fractional nonlinear modified Kawahara equation using the Homotopy Perturbation Sadik Transform, highlighting the effectiveness of semi-analytical techniques for nonlinear fractional models. Fractional models with special operators and geometrical settings have also been investigated. Ansari and Derakhshan [3] examined the time–space fractional Euler–Poisson–Darboux equation with Bessel fractional derivatives in both infinite and finite domains, addressing theoretical and numerical aspects of the problem. In the context of stochastic and financial models, several numerical frameworks have been proposed. Abdi-Mazraeh et al. [1] applied the multiple shooting method to solve the Black–Scholes equation, demonstrating improved numerical stability. Later, Abdi-Mazraeh et al. [2] constructed operational matrices based on linear cardinal B-spline functions to solve fractional stochastic integro-differential equations. Similarly, Irandoust-Pakchin et al. [28] employed flatlet oblique multiwavelets within a Galerkin framework for solving fractional stochastic integro-differential equations. In addition, Irandoust-Pakchin and Abdi-Mazraeh [27] derived explicit forms of fractional second linear multistep methods and performed a comprehensive

stability analysis. Overall, the above studies collectively contribute to the advancement of numerical analysis, stability theory, and high-accuracy computational schemes for fractional differential equations. They demonstrate the growing importance of distributed-order operators, Riesz-type derivatives, stochastic fractional models, and meshless or hybrid numerical techniques in modeling complex real-world phenomena.

The rest of this article is organized as follows; In section 2, we provide some key definitions and useful lemmas. Section 3 introduces two numerical approaches based on the radial basis function (RBF) collocation and the radial basis function-generated finite difference (RBF-FD) methods, which are applied to discretize the proposed model in the spatial variables. In section 4, we describe the implementation details of the GRBF and RBF-FD schemes for the GKdVB equation. Section 5 presents the stability analysis of the numerical method given in Eq. (4.4). Finally, section 6 concludes the paper.

2. Preliminary

This section introduces key definitions and practical lemmas that will be used in the next section for approximation, as well as for analyzing stability and convergence.

Definition 2.1. [21][Regularized Caputo–Prabhakar Derivative] The regularized Caputo–Prabhakar derivative of order β with parameters α, μ, ν is defined as

$$ {}^{C}\mathcal{D}^{\nu}_{\alpha,\beta,\mu} w(x,t) = \mathcal{E}^{-\nu}_{\alpha,\, n-\beta,\, \mu} \frac{d^n}{dt^n} w(x,t), \tag{2.1} $$

where $n = \lceil \beta \rceil$ is the smallest integer greater than or equal to β. The associated Prabhakar integral operator is given by

$$ \mathcal{E}^{-\nu}_{\alpha,\, n-\beta,\, \mu} w(x,t) = \int_0^t (t-\gamma)^{n-\beta-1} \mathbf{E}^{-\nu}_{\alpha,\, n-\beta,\, \mu}\big(\mu(t-\gamma)^{\alpha}\big)\, w(x,\gamma)\, d\gamma, \tag{2.2} $$

where $\alpha, \beta, \mu, \nu \in \mathbb{C}$ with $\Re(\alpha) > 0$ and $\Re(\beta) > 0$. In Eq. (2.2), the symbol $\mathbf{E}^{\nu}_{\alpha,\beta,\mu}(t)$ denotes the generalized Mittag–Leffler function [11], which is defined as

$$ \mathbf{E}^{\nu}_{\alpha,\beta,\mu}(t) = \sum_{l=0}^{\infty} \frac{\Gamma(\nu+l)}{\Gamma(\nu)\,\Gamma(\alpha l+\beta)\, l!}\, t^l, \tag{2.3} $$

where $\alpha, \beta, \mu, \nu \in \mathbb{C}$ and $\Gamma(\cdot)$ denotes the Gamma function.

Lemma 2.2. *Assume that $0 < \beta < 1$, $\alpha, \mu \in \mathbb{C}$, $\nu \in \mathbb{C}$, and $w(t) \in C^2[0, t_k]$. Then, the regularized Caputo–Prabhakar derivative displayed in Eq. (2.1), for $n = 1$, can be approximated using the L1-type discrete scheme as follows:*

$$ {}^{C}\mathcal{D}^{\nu}_{\alpha,\beta,\mu} w(t_k) \approx \sum_{m=1}^{k} A^{(\alpha,\beta,\mu,\nu)}_{k-m} \big(w(t_m) - w(t_{m-1})\big) + \mathcal{O}(\tau^{1-\beta}), \tag{2.4} $$

where the weights $A^{(\alpha,\beta,\mu,\nu)}_{k-m}$ are given by

$$ A^{(\alpha,\beta,\mu,\nu)}_{k-m} = \frac{1}{\tau}\Big[(t_k - t_{m-1})^{1-\beta} \mathbf{E}^{-\nu}_{\alpha,2-\beta,\mu}\big(\mu(t_k - t_{m-1})^{\alpha}\big) - (t_k - t_m)^{1-\beta} \mathbf{E}^{-\nu}_{\alpha,2-\beta,\mu}\big(\mu(t_k - t_m)^{\alpha}\big)\Big], \tag{2.5} $$

and $\mathbf{E}^{\nu}_{\alpha,\beta,\mu}(t)$ denotes the generalized Mittag–Leffler function defined in Eq. (2.3).

Proof. We consider the regularized Caputo–Prabhakar derivative in Eq. (2.1) for $n = 1$ at the point $t = t_k$:

$$ {}^{C}\mathcal{D}^{\nu}_{\alpha,\beta,\mu} w(t_k) = \int_0^{t_k} (t_k - \gamma)^{-\beta} \mathbf{E}^{-\nu}_{\alpha,1-\beta,\mu}\big(\mu(t_k-\gamma)^{\alpha}\big) \frac{d}{d\gamma} w(\gamma)\, d\gamma. \tag{2.6} $$

We partition the interval $[0, t_k]$ into uniform subintervals of length τ, with nodes $t_m = m\tau$, $m = 0, 1, \ldots, k$. Then Eq. (2.6) can be written as

$$ {}^{C}\mathcal{D}^{\nu}_{\alpha,\beta,\mu} w(t_k) = \sum_{m=1}^{k} \int_{t_{m-1}}^{t_m} (t_k - \gamma)^{-\beta} \mathbf{E}^{-\nu}_{\alpha,1-\beta,\mu}\big(\mu(t_k-\gamma)^{\alpha}\big) w'(\gamma)\, d\gamma. \tag{2.7} $$

On each subinterval $[t_{m-1}, t_m]$, the derivative $w'(\gamma)$ is approximated by the first-order difference

$$w'(\gamma) = \frac{w(t_m) - w(t_{m-1})}{\tau} + R_m(\gamma), \tag{2.8}$$

where, since $w \in C^2[0, t_k]$, the remainder satisfies

$$|R_m(\gamma)| \le C\tau, \qquad \gamma \in [t_{m-1}, t_m].$$

Substituting Eq. (2.8) into Eq. (2.7) yields

$$\begin{aligned} {}^{C}\mathcal{D}^{\nu}_{\alpha,\beta,\mu} w(t_k) = &\sum_{m=1}^{k} \frac{w(t_m) - w(t_{m-1})}{\tau} \int_{t_{m-1}}^{t_m} (t_k - \gamma)^{-\beta} \mathbf{E}^{-\nu}_{\alpha,1-\beta,\mu}\big(\mu(t_k - \gamma)^{\alpha}\big)\, d\gamma \\ &+ \sum_{m=1}^{k} \int_{t_{m-1}}^{t_m} (t_k - \gamma)^{-\beta} \mathbf{E}^{-\nu}_{\alpha,1-\beta,\mu}\big(\mu(t_k - \gamma)^{\alpha}\big) R_m(\gamma)\, d\gamma. \end{aligned} \tag{2.9}$$

We define the discrete weights

$$A^{(\alpha,\beta,\mu,\nu)}_{k-m} = \frac{1}{\tau} \int_{t_{m-1}}^{t_m} (t_k - \gamma)^{-\beta} \mathbf{E}^{-\nu}_{\alpha,1-\beta,\mu}\big(\mu(t_k - \gamma)^{\alpha}\big)\, d\gamma. \tag{2.10}$$

Using the change of variables $s = t_k - \gamma$, Eq. (2.10) becomes

$$A^{(\alpha,\beta,\mu,\nu)}_{k-m} = \frac{1}{\tau} \int_{t_k - t_m}^{t_k - t_{m-1}} s^{-\beta} \mathbf{E}^{-\nu}_{\alpha,1-\beta,\mu}(\mu s^{\alpha})\, ds. \tag{2.11}$$

From the known integral identity of the generalized Mittag–Leffler function (see [30]),

$$\int s^{-\beta} \mathbf{E}^{-\nu}_{\alpha,1-\beta,\mu}(\mu s^{\alpha})\, ds = s^{1-\beta} \mathbf{E}^{-\nu}_{\alpha,2-\beta,\mu}(\mu s^{\alpha}), \tag{2.12}$$

we obtain

$$A^{(\alpha,\beta,\mu,\nu)}_{k-m} = \frac{1}{\tau}\Big[(t_k - t_{m-1})^{1-\beta} \mathbf{E}^{-\nu}_{\alpha,2-\beta,\mu}(\mu(t_k - t_{m-1})^{\alpha}) - (t_k - t_m)^{1-\beta} \mathbf{E}^{-\nu}_{\alpha,2-\beta,\mu}(\mu(t_k - t_m)^{\alpha})\Big]. \tag{2.13}$$

Finally, we estimate the truncation error. Using $|R_m(\gamma)| \le C\tau$ and the boundedness of the generalized Mittag–Leffler function on $[0, t_k]$, we obtain

$$|\text{Error}| \le C\tau \int_0^{t_k} (t_k - \gamma)^{-\beta}\, d\gamma = C\tau \frac{t_k^{1-\beta}}{1-\beta}.$$

Taking into account the weak singularity of the kernel and the accumulation of local quadrature errors over the uniform partition, one obtains the classical L1-type estimate

$$\text{Error} = \mathcal{O}(\tau^{1-\beta}),$$

which is consistent with the standard error analysis of the L1 approximation for Caputo-type fractional derivatives. This completes the proof. □

Lemma 2.3 (Nonlinear term approximation)**.** *For $p = 1, 2, \ldots$, the nonlinear term $(w^p w_x)^{n+1}$ can be approximated as*

$$(w^p w_x)^{n+1} \approx (w^p)^n w_x^{n+1} + p(w^{p-1})^n w_x^n w^{n+1} - p(w^p)^n w_x^n. \tag{2.14}$$

Proof. Using a Taylor expansion in time, we have

$$(w^p w_x)^{n+1} = (w^p w_x)(x, t_{n+1}) = (w^p w_x)(x, t_n) + \tau \frac{\partial (w^p w_x)}{\partial t}(x, t_n) + \mathcal{O}(\tau^2), \tag{2.15}$$

where τ is the time step. Expanding the time derivative gives

$$\frac{\partial (w^p w_x)}{\partial t} = p w^{p-1} w_x w_t + w^p w_{xt}. \tag{2.16}$$

Substituting Eq. (2.16) into Eq. (2.15) and using the finite difference approximations for w_t and w_{xt}, we obtain

$$(w^p w_x)^{n+1} = (w^p)^n w_x^{n+1} + p(w^{p-1})^n w_x^n w^{n+1} - p(w^p)^n w_x^n + \mathcal{O}(\tau^2). \tag{2.17}$$

□

3. Collocation techniques

In this section, we introduce and examine two numerical approaches based on the radial basis function (RBF) collocation and the radial basis function–generated finite difference (RBF-FD) that will be used to discretize the proposed model with respect to spatial variables. Both methods are described in detail in the following subsections.

3.1. Radial Basis Function Collocation.

We consider a set of $\mathcal{N}$ distinct points in $\mathbb{R}^d$, denoted as

$$X = \{x_1, x_2, \ldots, x_{\mathcal{N}}\}.$$

At each of these points, the value of a function $w(x)$ is known, and we write this as

$$w_j = w(x_j), \quad j = 1, 2, \ldots, \mathcal{N}.$$

To approximate the function $w(x)$, we use a combination of RBFs and polynomial terms. Then approximation of the function $w(x)$ is computed as follows:

$$w(x) \approx \vartheta(x, \varepsilon) = \sum_{i=1}^{\mathcal{N}} \rho_i \, \Phi(\|x - x_i\|, \varepsilon) + \sum_{k=1}^{m} \rho_{\mathcal{N}+k} \, q_k(x). \tag{3.1}$$

Here, $\Phi(\|x - x_j\|, \varepsilon)$ is a radial function that depends on the distance between x and x_j, as well as a parameter ε that controls its shape. The functions $q_k(x)$ are polynomials of degree up to $\mathcal{Q}$, chosen to form a suitable basis. The coefficients ρ_i and $\rho_{\mathcal{N}+k}$ are unknowns that will be determined during the approximation process. The unknown coefficients ρ_i and $\rho_{\mathcal{N}+k}$ are obtained by enforcing the interpolation conditions, which require the approximation to exactly match the known function values at the data points. Thus, for each $i = 1, 2, \ldots, \mathcal{N}$, we have

$$\vartheta(x_i, \varepsilon) = w_i, \quad j = 1, 2, \ldots, \mathcal{N}. \tag{3.2}$$

This formulation produces a system of linear equations for the coefficients, which can then be solved to obtain an approximate representation of $w(x)$ over the domain. The augmented polynomial terms are included with the following constraints:

$$\sum_{i=1}^{\mathcal{N}} \rho_i \, q_k(x_i) = 0, \quad k = 1, \ldots, m. \tag{3.3}$$

Combining Eq. (3.3) with the collocation conditions in Eq. (3.2) yields a linear system of the form

$$\mathbf{B}\,\boldsymbol{\rho} = \mathbf{g}, \tag{3.4}$$

in which

$$\mathbf{B} = \begin{bmatrix} \mathcal{P}_\Phi & Q \\ Q^\top & 0 \end{bmatrix}, \quad \boldsymbol{\rho} = \begin{bmatrix} \rho_1 \\ \vdots \\ \rho_{\mathcal{N}} \\ \vdots \\ \vdots \\ \rho_{\mathcal{N}+m} \end{bmatrix}, \quad \mathbf{g} = \begin{bmatrix} w_1 \\ \vdots \\ w_{\mathcal{N}} \\ 0 \\ \vdots \\ 0 \end{bmatrix}.$$

Here, the matrices $\mathcal{P}$ and Q are defined as follows:

$$\mathcal{P}_\Phi = \begin{bmatrix} \Phi(\|x_1 - x_1\|, \varepsilon) & \Phi(\|x_1 - x_2\|, \varepsilon) & \cdots & \Phi(\|x_1 - x_\mathcal{N}\|, \varepsilon) \\ \Phi(\|x_2 - x_1\|, \varepsilon) & \Phi(\|x_2 - x_2\|, \varepsilon) & \cdots & \Phi(\|x_2 - x_\mathcal{N}\|, \varepsilon) \\ \vdots & \vdots & \ddots & \vdots \\ \Phi(\|x_\mathcal{N} - x_1\|, \varepsilon) & \Phi(\|x_\mathcal{N} - x_2\|, \varepsilon) & \cdots & \Phi(\|x_\mathcal{N} - x_\mathcal{N}\|, \varepsilon) \end{bmatrix}, \quad Q = \begin{bmatrix} q_1(x_1) & \cdots & q_m(x_1) \\ q_1(x_2) & \cdots & q_m(x_2) \\ \vdots & \ddots & \vdots \\ q_1(x_\mathcal{N}) & \cdots & q_m(x_\mathcal{N}) \end{bmatrix}.$$

3.2. **RBF-FD Collocation Method.** The RBF-FD method is a mesh-free extension of the classical FD technique. In this method, the derivative of a function at a node x_i is approximated by a weighted sum of the function values at nearby nodes, forming a local stencil. Unlike conventional FD schemes that rely on polynomials, RBF-FD uses RBFs, which provide higher accuracy and greater flexibility for irregularly distributed nodes. Let $x_i \in X$ and define a stencil $S_i = \{x_{i_1}, x_{i_2}, \ldots, x_{i_{n_i}}\}$ around x_i. For a linear differential operator L, we seek weights $\varpi = (\varpi_1, \varpi_2, \ldots, \varpi_{n_i})$ such that

$$L(w(x_i)) \approx \sum_{l=1}^{n_i} \varpi_l \, w(x_{i_l}), \tag{3.5}$$

where x_i is the central node of the stencil $\mathbf{S}_i$. To compute the weights ϖ_l in Eq. (3.5), the operator L is applied to the RBFs centered at the stencil nodes, $\Phi_{i_l}(x) = \Phi(\|x - x_{i_l}\|)$, together with the polynomials $1, x, \ldots, x^m$ if exactness for polynomials up to degree m is desired. This leads to the linear system

$$\begin{bmatrix} \Phi(\|x_{i_1} - x_{i_1}\|, \varepsilon) & \Phi(\|x_{i_2} - x_{i_1}\|, \varepsilon) & \ldots & \Phi(\|x_{i_{n_i}} - x_{i_1}\|, \varepsilon) & 1 & x_{i_1} & \ldots & x_{i_1}^m \\ \Phi(\|x_{i_1} - x_{i_2}\|, \varepsilon) & \Phi(\|x_{i_2} - x_{i_2}\|, \varepsilon) & \ldots & \Phi(\|x_{i_{n_i}} - x_{i_2}\|, \varepsilon) & 1 & x_{i_2} & \ldots & x_{i_2}^m \\ \vdots & \vdots & \ddots & \vdots & \vdots & \vdots & \ddots & \vdots \\ \Phi(\|x_{i_1} - x_{n_i}\|, \varepsilon) & \Phi(\|x_{i_2} - x_{n_i}\|, \varepsilon) & \ldots & \Phi(\|x_{i_{n_i}} - x_{n_i}\|, \varepsilon) & 1 & x_{i_{n_i}} & \ldots & x_{i_{n_i}}^m \\ 1 & 1 & \ldots & 1 & 0 & 0 & \ldots & 0 \\ x_{i_1} & x_{i_2} & \ldots & x_{i_{n_i}} & 0 & 0 & \ldots & 0 \\ \vdots & \vdots & & \vdots & \vdots & \vdots & \ddots & \vdots \\ x_{i_1}^m & x_{i_2}^m & \ldots & x_{i_{n_i}}^m & 0 & 0 & \ldots & 0 \end{bmatrix} \begin{bmatrix} \varpi_1 \\ \varpi_2 \\ \vdots \\ \varpi_{n_i} \\ v_1 \\ \vdots \\ v_m \end{bmatrix}$$

$$= \begin{bmatrix} L\Phi(\|x - x_1\|, \varepsilon)\big|_{x=x_i} \\ L\Phi(\|x - x_2\|, \varepsilon)\big|_{x=x_i} \\ \vdots \\ L\Phi(\|x - x_{n_i}\|, \varepsilon)\big|_{x=x_i} \\ L1\big|_{x=x_i} \\ Lx\big|_{x=x_i} \\ \vdots \\ Lx^m\big|_{x=x_i} \end{bmatrix}. \tag{3.6}$$

Solving this system yields the weights $\varpi_1, \ldots, \varpi_{n_i}$ used in Eq. (3.5). The coefficients $v_1, \ldots, v_m$ act as auxiliary terms to enforce polynomial exactness, introducing at most minor approximation errors. For many commonly used RBFs, the matrix is non-singular, guaranteeing a unique solution.

4. Description of the methods

In this section, we describe the implementation details of the RBF–FD and GRBF methods for the GKdVB equation. Firstly, we discretize the time interval $[0, T]$ with a step size τ such that

$$t_0 = 0, \quad t_n = t_{n-1} + \tau = n\tau, \quad n = 1, 2, \ldots, m = \frac{T}{\tau}.$$

We then apply a finite difference approximation which is obtained in Lemma 2.2, along with the θ–weighted method ($0 \le \theta \le 1$) between two consecutive time steps t_n and t_{n+1} to Eq. (1.1), which can be written as:

$$\sum_{p=1}^{m} A_{m-n-1}^{(\alpha,\beta,\mu,\nu)}\left(w^{n+1}-w^{n}\right)+\theta\left(\xi\, w\, w_x+\eta\, w^2 w_x+\varrho\, w_{xx}+\sigma\, w_{xxx}\right)^{n+1} + (1-\theta)\left(\xi\, w\, w_x+\eta\, w^2 w_x+\varrho\, w_{xx}+\sigma\, w_{xxx}\right)^{n}=0, \tag{4.1}$$

where $w^n = w(x,t_n)$ for $n = 0,1,\ldots,m$, τ is the time step size, and $A_{m-n-1}^{(\alpha,\beta,\mu,\nu)}$ are the coefficients arising from the discretization of the time derivative which is obtained in Lemma 2.2. Applying Lemma 2.3 for $p=1$ and $p=2$, the nonlinear terms in Eq. (4.1) can be linearized as

$$\begin{aligned} p=1:&\quad (ww_x)^{n+1} = w^n w_x^{n+1} + w^{n+1} w_x^n - w^n w_x^n,\\ p=2:&\quad (w^2 w_x)^{n+1} = (w^2)^n w_x^{n+1} + 2w^n w_x^n w^{n+1} - 2(w^2)^n w_x^n. \end{aligned} \tag{4.2}$$

Substituting Eq. (4.2) into Eq. (4.1) and rearranging terms yields:

$$\begin{aligned} &\sum_{p=1}^{m} A_{m-n-1}^{(\alpha,\beta,\mu,\nu)}\left(w^{n+1}-w^{n}\right)+\theta\Big[\xi\big(w^n w_x^{n+1}+w^{n+1}w_x^n-w^n w_x^n\big)\\ &+\eta\big((w^2)^n w_x^{n+1}+2w^n w_x^n w^{n+1}-2(w^2)^n w_x^n\big)+\varrho\, w_{xx}^{n+1}+\sigma\, w_{xxx}^{n+1}\Big]\\ &+(1-\theta)\Big(\xi\, w^n w_x^n+\eta\,(w^n)^2 w_x^n+\varrho\, w_{xx}^n+\sigma\, w_{xxx}^n\Big)=0. \end{aligned} \tag{4.3}$$

So the above equation can be rewritten as follows:

$$\begin{aligned} &\left[\sum_{m=1}^{k} A_{k-m}^{(\alpha,\beta,\mu,\nu)}+\theta\big(\xi w_x^n+2\eta w^n w_x^n\big)\right] w^{n+1}+\theta\big(\xi w^n+\eta (w^n)^2\big) w_x^{n+1}+\theta\,\varrho\, w_{xx}^{n+1}+\theta\,\sigma\, w_{xxx}^{n+1}\\ &=\sum_{m=1}^{k} A_{k-m}^{(\alpha,\beta,\mu,\nu)} w^n-(1-\theta)\big(\xi w^n w_x^n+\eta (w^n)^2 w_x^n+\varrho\, w_{xx}^n+\sigma\, w_{xxx}^n\big)-\theta\big(-w^n w_x^n\,\xi-2(w^n)^2 w_x^n\,\eta\big). \end{aligned} \tag{4.4}$$

4.1. **Implementation of the RBF-FD Method.** We begin by selecting $\mathcal{N}$ distinct points $X=\{x_1,x_2,\ldots,x_{\mathcal{N}}\}$ in the domain $\Omega=[a,b]$, where x_i, $i=2,\ldots,\mathcal{N}-1$ are interior points, and x_1 and $x_{\mathcal{N}}$ are boundary points. For each point x_i, a local stencil is formed as

$$\mathbf{S}_i=\{x_{i_1},x_{i_2},\ldots,x_{i_{n_i}}\}=\{x_j\in X:\|x_j-x_i\|\le R\},$$

where R is the support radius. Without loss of generality, we assume $x_i=x_{i_1}$. The weights for the differential operators $\frac{\partial}{\partial x}$, $\frac{\partial^2}{\partial x^2}$, and $\frac{\partial^3}{\partial x^3}$ at the interior node x_i are computed using Eq. (3.6). Therefore, the approximate first, second, and third order derivatives of the function w are calculated as follows:

$$\begin{aligned} w_x(x_i)&\approx \varpi_{i_1}^{x} w_{i_1}+\varpi_{i_2}^{x} w_{i_2}+\cdots+\varpi_{i_{n_i}}^{x} w_{i_{n_i}},\\ w_{xx}(x_i)&\approx \varpi_{i_1}^{xx} w_{i_1}+\varpi_{i_2}^{xx} w_{i_2}+\cdots+\varpi_{i_{n_i}}^{xx} w_{i_{n_i}},\\ w_{xxx}(x_i)&\approx \varpi_{i_1}^{xxx} w_{i_1}+\varpi_{i_2}^{xxx} w_{i_2}+\cdots+\varpi_{i_{n_i}}^{xxx} w_{i_{n_i}}. \end{aligned} \tag{4.5}$$

By applying the collocation procedure to the interior points in Eq. (4.4) and substituting the derivatives using Eq. (4.5), we obtain a linear system of equations that can be solved for the unknown nodal values. Then

$$\begin{aligned}
&\left[\sum_{m=1}^{k} A_{k-m}^{(\alpha,\beta,\mu,\nu)} + \theta\Big(\xi \sum_{j=1}^{n_i} \varpi_{i_j}^{x} w_{i_j}^{n} + 2\eta w^{n} \sum_{j=1}^{n_i} \varpi_{i_j}^{x} w_{i_j}^{n}\Big)\right] w^{n+1} \\
&+ \theta\Big(\xi w^{n} + \eta (w^{n})^{2}\Big) \sum_{j=1}^{n_i} \varpi_{i_j}^{x} w_{i_j}^{n+1} + \theta\varrho \sum_{j=1}^{n_i} \varpi_{i_j}^{xx} w_{i_j}^{n+1} + \theta\sigma \sum_{j=1}^{n_i} \varpi_{i_j}^{xxx} w_{i_j}^{n+1} \\
&= \sum_{m=1}^{k} A_{k-m}^{(\alpha,\beta,\mu,\nu)} w^{n} - (1-\theta)\Big(\xi w^{n} \sum_{j=1}^{n_i} \varpi_{i_j}^{x} w_{i_j}^{n} + \eta (w^{n})^{2} \sum_{j=1}^{n_i} \varpi_{i_j}^{x} w_{i_j}^{n} + \varrho \sum_{j=1}^{n_i} \varpi_{i_j}^{xx} w_{i_j}^{n} + \sigma \sum_{j=1}^{n_i} \varpi_{i_j}^{xxx} w_{i_j}^{n}\Big) \\
&- \theta\Big(\xi w^{n} \sum_{j=1}^{n_i} \varpi_{i_j}^{x} w_{i_j}^{n} + 2\eta (w^{n})^{2} \sum_{j=1}^{n_i} \varpi_{i_j}^{x} w_{i_j}^{n}\Big).
\end{aligned} \tag{4.6}$$

To solve the discrete problem given in Eq. (4.6), we reformulate it as a linear algebraic system. For this purpose, we introduce the following notations:

$$c_{n,i}^{x} = \sum_{j=1}^{n_i} \varpi_{i_j}^{x}\, w_{i_j}^{n},\; c_{n,i}^{xx} = \sum_{j=1}^{n_i} \varpi_{i_j}^{xx}\, w_{i_j}^{n},\; c_{n,i}^{xxx} = \sum_{j=1}^{n_i} \varpi_{i_j}^{xxx}\, w_{i_j}^{n}, \tag{4.7}$$

and

$$d_i^{n} = \xi\, w_i^{n} + \eta\, (w_i^{n})^{2}. \tag{4.8}$$

Also, we define the accumulated convolution weight as follows:

$$S_k = \sum_{m=1}^{k} A_{k-m}^{(\alpha,\beta,\mu,\nu)}. \tag{4.9}$$

By substituting Eq. (4.7) into Eq. (4.6) and collocating all interior nodes, we obtain a linear system of equations in the unknown vector as follows:

$$A\, W^{\,n+1} = b, \tag{4.10}$$

in which

$$W^{\,n+1} = \big[w_2^{n+1},\; w_3^{n+1},\; \ldots,\; w_{N-1}^{n+1}\big]^{T}.$$

The coefficient matrix $A \in \mathbb{R}^{(N-2)\times(N-2)}$ is sparse, with nonzero entries arising only from the discretization stencils. The diagonal entries are obtained for $i = 2, \ldots, N-1$ and take the form

$$a_{(i-1)(i-1)} = S_k + \theta\Big(\xi\, c_{n,i}^{x} + 2\eta\, w_i^{n}\, c_{n,i}^{x}\Big) + \theta\, d_i^{n}\, \varpi_{i_1}^{x} + \theta\, \varrho\, \varpi_{i_1}^{xx} + \theta\, \sigma\, \varpi_{i_1}^{xxx}. \tag{4.11}$$

The off-diagonal entries, corresponding to neighboring nodes in the stencil, are given for $j = 2, \ldots, n_i$ with $ij \neq 1, N$ by

$$a_{(i-1)(ij-1)} = \theta\, d_i^{n}\, \varpi_{i_j}^{x} + \theta\, \varrho\, \varpi_{i_j}^{xx} + \theta\, \sigma\, \varpi_{i_j}^{xxx}, \tag{4.12}$$

while all remaining components of A vanish. The right-hand side vector $b \in \mathbb{R}^{(N-2)}$ is constructed consistently with the discretization. For each $i = 2, \ldots, N-1$, the corresponding entry is written as

$$b_{i-1} = S_k\, w_i^{n} - (1-\theta)\Big(\xi\, w_i^{n}\, c_{n,i}^{x} + \eta\, (w_i^{n})^{2}\, c_{n,i}^{x} + \varrho\, c_{n,i}^{xx} + \sigma\, c_{n,i}^{xxx}\Big) - \theta\Big(\xi\, w_i^{n}\, c_{n,i}^{x} + 2\eta\, (w_i^{n})^{2}\, c_{n,i}^{x}\Big). \tag{4.13}$$

A special treatment is required when the stencil $\mathbf{S}_i$ involves boundary nodes, i.e., when $i_j = 1$ or $i_j = N$. In such cases, the associated unknowns $w_{i_j}^{n+1}$ are prescribed by the boundary conditions and thus do not belong to the set

of free variables. Consequently, their contribution is transferred from the left-hand side to the right-hand side of the system. More precisely, the following correction is applied:

$$b_{i-1} \;\leftarrow\; b_{i-1} - a_{(i-1)(i_j-1)}\, w_{i_j}^{n+1}, \tag{4.14}$$

after which the corresponding coefficient $a_{(i-1)(i_j-1)}$ in the matrix A is set to zero.

4.2. **GRBF Implementation Details.** We select $\mathcal{N}$ distinct points x_i, $i = 1, \ldots, \mathcal{N}$ in the domain $\Omega = [a, b]$, where the points x_i for $i = 2, \ldots, \mathcal{N}-1$ represent the interior nodes, and x_1 and $x_{\mathcal{N}}$ correspond to the boundary nodes. The approximate solution at time t_{n+1} is expressed as

$$w(x, t_{n+1}) \approx w^{n+1}(x) = \sum_{j=1}^{\mathcal{N}} \rho_j^{n+1}\, \Phi_j(x) + \rho_{\mathcal{N}+1}^{n+1}\, x + \rho_{\mathcal{N}+2}^{n+1}, \tag{4.15}$$

where $\Phi_j(x) = \Phi(\|x - x_j\|)$ are the chosen RBFs, and ρ_j^{n+1}, $j = 1, \ldots, \mathcal{N}+2$, are the unknown coefficients to be determined. By substituting the approximation (4.15) into Eqs. (4.4) and (1.3), and applying collocation at the nodes $x_1, \ldots, x_{\mathcal{N}}$, one obtains a system of equations for the coefficients ρ_j^{n+1}. This system fully enforces the governing equations at the collocation points, including the boundary conditions at x_1 and $x_{\mathcal{N}}$. Thus

$$\begin{aligned}
&\Big[\sum_{m=1}^{k} A_{k-m}^{(\alpha,\beta,\mu,\nu)} + \theta\Big(\xi\Big(\sum_{j=1}^{\mathcal{N}} \rho_j^n \Phi_j'(x_i) + \rho_{\mathcal{N}+1}^n\Big) + 2\eta\Big(\sum_{j=1}^{\mathcal{N}} \rho_j^n \Phi_j(x_i) + \rho_{\mathcal{N}+1}^n x_i + \rho_{\mathcal{N}+2}^n\Big)\Big(\sum_{j=1}^{\mathcal{N}} \rho_j^n \Phi_j'(x_i) + \rho_{\mathcal{N}+1}^n\Big)\Big)\Big] \\
&\quad \times \Big(\sum_{j=1}^{\mathcal{N}} \rho_j^{n+1} \Phi_j(x_i) + \rho_{\mathcal{N}+1}^{n+1} x_i + \rho_{\mathcal{N}+2}^{n+1}\Big)\theta\Big(\xi\Big(\sum_{j=1}^{\mathcal{N}} \rho_j^n \Phi_j(x_i) + \rho_{\mathcal{N}+1}^n x_i + \rho_{\mathcal{N}+2}^n\Big) \\
&\quad + \eta\Big(\sum_{j=1}^{\mathcal{N}} \rho_j^n \Phi_j(x_i) + \rho_{\mathcal{N}+1}^n x_i + \rho_{\mathcal{N}+2}^n\Big)^2\Big)\Big(\sum_{j=1}^{\mathcal{N}} \rho_j^{n+1} \Phi_j'(x_i) + \rho_{\mathcal{N}+1}^{n+1}\Big) + \theta\, \varrho \sum_{j=1}^{\mathcal{N}} \rho_j^{n+1} \Phi_j''(x_i) + \theta\, \sigma \sum_{j=1}^{\mathcal{N}} \rho_j^{n+1} \Phi_j'''(x_i) \\
&\quad = \sum_{m=1}^{k} A_{k-m}^{(\alpha,\beta,\mu,\nu)} \Big(\sum_{j=1}^{\mathcal{N}} \rho_j^n \Phi_j(x_i) + \rho_{\mathcal{N}+1}^n x_i + \rho_{\mathcal{N}+2}^n\Big) - (1-\theta)\Big[\xi\Big(\sum_{j=1}^{\mathcal{N}} \rho_j^n \Phi_j(x_i) + \rho_{\mathcal{N}+1}^n x_i + \rho_{\mathcal{N}+2}^n\Big) \\
&\quad \times \Big(\sum_{j=1}^{\mathcal{N}} \rho_j^n \Phi_j'(x_i) + \rho_{\mathcal{N}+1}^n\Big) + \eta\Big(\sum_{j=1}^{\mathcal{N}} \rho_j^n \Phi_j(x_i) + \rho_{\mathcal{N}+1}^n x_i + \rho_{\mathcal{N}+2}^n\Big)^2\Big(\sum_{j=1}^{\mathcal{N}} \rho_j^n \Phi_j'(x_i) + \rho_{\mathcal{N}+1}^n\Big) \\
&\quad + \varrho \sum_{j=1}^{\mathcal{N}} \rho_j^n \Phi_j''(x_i) + \sigma \sum_{j=1}^{\mathcal{N}} \rho_j^n \Phi_j'''(x_i)\Big] - \theta\Big[-\xi\Big(\sum_{j=1}^{\mathcal{N}} \rho_j^n \Phi_j(x_i) + \rho_{\mathcal{N}+1}^n x_i + \rho_{\mathcal{N}+2}^n\Big)\Big(\sum_{j=1}^{\mathcal{N}} \rho_j^n \Phi_j'(x_i) + \rho_{\mathcal{N}+1}^n\Big) \\
&\quad - 2\eta\Big(\sum_{j=1}^{\mathcal{N}} \rho_j^n \Phi_j(x_i) + \rho_{\mathcal{N}+1}^n x_i + \rho_{\mathcal{N}+2}^n\Big)^2 \times \Big(\sum_{j=1}^{\mathcal{N}} \rho_j^n \Phi_j'(x_i) + \rho_{\mathcal{N}+1}^n\Big)\Big].
\end{aligned} \tag{4.16}$$

with the boundary conditions and additional constraints

$$\begin{aligned}
&\sum_{j=1}^{\mathcal{N}} \rho_j^{n+1}\, \Phi_j(x_1) + \rho_{\mathcal{N}+1}^{n+1} x_1 + \rho_{\mathcal{N}+2}^{n+1} = f_1(t_{n+1}), \\
&\sum_{j=1}^{\mathcal{N}} \rho_j^{n+1}\, \Phi_j(x_N) + \rho_{\mathcal{N}+1}^{n+1} x_N + \rho_{\mathcal{N}+2}^{n+1} = f_2(t_{n+1}), \\
&\sum_{j=1}^{\mathcal{N}} \rho_j^{n+1}\, x_j = 0, \\
&\sum_{j=1}^{\mathcal{N}} \rho_j^{n+1} = 0.
\end{aligned} \tag{4.17}$$

Equations (4.16) and (4.17) yield a $(\mathcal{N}+2)\times(\mathcal{N}+2)$ system of linear equations in the following matrix form:

$$\underbrace{\begin{bmatrix} \theta\Big[\xi D_1^n + 2\eta\,(w^n \circ D_1^n)\Big] & \theta\Big[\xi w^n + \eta (w^n)^2\Big] & \theta D_2 & \theta D_3 & \\ \Phi_1(x_1) & \cdots & \Phi_{\mathcal{N}}(x_1) & x_1 & 1 \\ \Phi_1(x_{\mathcal{N}}) & \cdots & \Phi_{\mathcal{N}}(x_{\mathcal{N}}) & x_{\mathcal{N}} & 1 \\ x_1 & \cdots & x_{\mathcal{N}} & 0 & 0 \\ 1 & \cdots & 1 & 0 & 0 \end{bmatrix}}_{H} \underbrace{\begin{bmatrix} \rho_1^{n+1} \\ \vdots \\ \rho_{\mathcal{N}}^{n+1} \\ \rho_{\mathcal{N}+1}^{n+1} \\ \rho_{\mathcal{N}+2}^{n+1} \end{bmatrix}}_{\boldsymbol{\rho}^{n+1}}$$

$$= \underbrace{\begin{bmatrix} \displaystyle\sum_{m=1}^{k} A_{k-m}^{(\alpha,\beta,\mu,\nu)}\, w^n - (1-\theta)\Big[\xi\, w^n \circ D_1^n + \eta (w^n)^2 \circ D_1^n + \varrho D_2\, \rho^n + \sigma D_3\, \rho^n\Big] \\ f_1(t_{n+1}) \\ f_2(t_{n+1}) \\ 0 \\ 0 \end{bmatrix}}_{\mathbf{b}}, \tag{4.18}$$

with the boundary conditions and additional constraints

$$\sum_{j=1}^{\mathcal{N}} \rho_j^{n+1}\, \Phi_j(x_1) + \rho_{\mathcal{N}+1}^{n+1} x_1 + \rho_{\mathcal{N}+2}^{n+1} = f_1(t_{n+1}),$$

$$\sum_{j=1}^{\mathcal{N}} \rho_j^{n+1}\, \Phi_j(x_{\mathcal{N}}) + \rho_{\mathcal{N}+1}^{n+1} x_{\mathcal{N}} + \rho_{\mathcal{N}+2}^{n+1} = f_2(t_{n+1}),$$

$$\sum_{j=1}^{\mathcal{N}} \rho_j^{n+1}\, x_j = 0, \quad \sum_{j=1}^{\mathcal{N}} \rho_j^{n+1} = 0.$$

in which

$$w^n(x_i) = \sum_{j=1}^{\mathcal{N}} \rho_j^n\, \Phi_j(x_i) + \rho_{\mathcal{N}+1}^n\, x_i + \rho_{\mathcal{N}+2}^n,$$

$$D_1^n(x_i) = \sum_{j=1}^{\mathcal{N}} \rho_j^n\, \Phi_j'(x_i) + \rho_{\mathcal{N}+1}^n,$$

$$D_2(x_i) = \sum_{j=1}^{\mathcal{N}} \rho_j^{n+1}\, \Phi_j''(x_i),$$

$$D_3(x_i) = \sum_{j=1}^{\mathcal{N}} \rho_j^{n+1}\, \Phi_j'''(x_i),$$

$$w^{n+1}(x_i) = \sum_{j=1}^{\mathcal{N}} \rho_j^{n+1}\, \Phi_j(x_i) + \rho_{\mathcal{N}+1}^{n+1} x_i + \rho_{\mathcal{N}+2}^{n+1}.$$

The system of $(\mathcal{N}+2)\times(\mathcal{N}+2)$ linear equations given by Eq. (4.18) as

$$H\,\rho^{n+1} = \mathbf{b},$$

can be solved using direct method.

5. Stability Analysis

In this section, we present the stability analysis of the numerical method given in Eq. (4.4). Following the standard approach in nonlinear stability analysis, we freeze the nonlinear coefficients locally by setting

$$w^n = W, \qquad w_x^n = W_x, \tag{5.1}$$

where W and W_x are regarded as constants during the analysis. It should be emphasized that this frozen–coefficient assumption yields a local linearized stability result rather than a full nonlinear guarantee. The derived condition ensures boundedness of small perturbations around the reference state (W, W_x) for sufficiently small temporal and spatial discretization parameters, but it does not imply unconditional stability of the fully nonlinear problem. For convenience, we introduce the following notations:

$$S = \sum_{m=1}^{k} A_{k-m}^{(\alpha,\beta,\mu,\nu)}, \quad A = \xi W_x + 2\eta W W_x, \quad B = \xi W + \eta W^2. \tag{5.2}$$

Substituting (5.1)–(5.2) into (4.4) yields the following frozen-coefficient equation:

$$\begin{aligned}\big(S + \theta A\big)w^{n+1} + \theta B\, w_x^{n+1} + \theta\varrho\, w_{xx}^{n+1} + \theta\sigma\, w_{xxx}^{n+1} = \big(S + (2\theta-1)\xi W W_x + (3\theta-1)\eta W^2 W_x\big)w^n \\ + (1-\theta)\,\varrho\, w_{xx}^n + (1-\theta)\,\sigma\, w_{xxx}^n.\end{aligned} \tag{5.3}$$

To carry out von Neumann stability analysis, we assume a Fourier mode solution of the form

$$w_j^n = \zeta^n e^{i\kappa x_j}, \tag{5.4}$$

where κ is the wave number and ζ is the amplification factor. For a Fourier mode of this form, the spatial derivatives can be represented as

$$w_x \mapsto i\kappa, \quad w_{xx} \mapsto -\kappa^2, \quad w_{xxx} \mapsto -i\kappa^3. \tag{5.5}$$

Substituting (5.4)–(5.5) into (5.3), we obtain

$$\big(\alpha_2 + i\beta_2\big)\,\zeta^{\,n+1} = \big(\alpha_1 + i\beta_1\big)\,\zeta^n, \tag{5.6}$$

which implies

$$\zeta = \frac{\alpha_1 + i\beta_1}{\alpha_2 + i\beta_2}. \tag{5.7}$$

The coefficients $\alpha_1, \beta_1, \alpha_2, \beta_2$ in Eq. (5.7) are given by

$$\begin{aligned}&\alpha_2 = S + \theta A - \theta\varrho\kappa^2, \quad \beta_2 = \theta\big(B\kappa - \sigma\kappa^3\big), \\ &\alpha_1 = S + (2\theta-1)\,\xi W W_x + (3\theta-1)\,\eta W^2 W_x + (1-\theta)\varrho\kappa^2, \quad \beta_1 = (1-\theta)\sigma\kappa^3.\end{aligned} \tag{5.8}$$

The squared modulus of the amplification factor is obtained as follows:

$$|\zeta|^2 = \frac{\alpha_1^2 + \beta_1^2}{\alpha_2^2 + \beta_2^2} = \frac{N}{D}, \qquad N = \alpha_1^2 + \beta_1^2, \quad D = \alpha_2^2 + \beta_2^2. \tag{5.9}$$

For stability, we require $|\zeta| \le 1$ for all κ. A sufficient condition is

$$D - N \ge 0, \tag{5.10}$$

which ensures that $|\zeta| \le 1$. Then,

$$\begin{aligned}D - N &= (\alpha_2^2 + \beta_2^2) - (\alpha_1^2 + \beta_1^2) \\ &= (\alpha_2 - \alpha_1)(\alpha_2 + \alpha_1) + (\beta_2 - \beta_1)(\beta_2 + \beta_1).\end{aligned} \tag{5.11}$$

Thus

$$\begin{aligned}
&\alpha_2 - \alpha_1 = S + \theta A - \theta\varrho\kappa^2 - \left[S + (2\theta-1)A + (1-\theta)\varrho\kappa^2\right] = (1-2\theta)A - \varrho\kappa^2,\\
&\alpha_2 + \alpha_1 = 2S + (3\theta-1)A,\\
&\beta_2 - \beta_1 = \theta(B\kappa - \sigma\kappa^3) - (1-\theta)(B\kappa - \sigma\kappa^3) = (2\theta-1)(B\kappa - \sigma\kappa^3),\\
&\beta_2 + \beta_1 = (B\kappa - \sigma\kappa^3).
\end{aligned} \tag{5.12}$$

Substituting Eqs. (5.12) into Eq. (5.11), we obtain

$$\begin{aligned}
D - N &= (\alpha_2 - \alpha_1)(\alpha_2 + \alpha_1) + (\beta_2 - \beta_1)(\beta_2 + \beta_1)\\
&= \left[(1-2\theta)A - \varrho\kappa^2\right]\left[2S + (3\theta-1)A\right] + (2\theta-1)(B\kappa - \sigma\kappa^3)^2\\
&= (2\theta-1)(2AS + (3\theta-1)A^2 + (B\kappa - \sigma\kappa^3)^2) - 2\varrho\kappa^2 S - (3\theta-1)\varrho\kappa^2 A.
\end{aligned} \tag{5.13}$$

Since $\varrho \le 0$, $S > 0$ (sum of coefficients), and $\theta \ge 1/2$, each term in $D - N$ is nonnegative, then , we conclude that

- The term $(2\theta-1)(B\kappa - \sigma\kappa^3)^2 \ge 0$,
- The term $-\varrho\kappa^2(2S + (3\theta-1)A) \ge 0$,
- The term $(2\theta-1)A(2S + (3\theta-1)A) \ge 0$ if $A \ge 0$.

A direct expansion of $D - N$ shows that the dominant terms are nonnegative when

$$\theta \ge \tfrac{1}{2}, \qquad \varrho \le 0, \qquad A = \xi W_x + 2\eta W W_x \ge 0. \tag{5.14}$$

Therefore, condition (5.14) guarantees that the amplification factor satisfies $|\zeta| \le 1$ for all κ, thereby establishing the linear stability of the scheme (4.4).

5.0.1. *Fully Discrete Stability Analysis.* In this subsection, the stability of the fully discrete numerical scheme is investigated. The time discretization of the Prabhakar-type Caputo derivative is obtained using a convolution formula of second–order accuracy. For the temporal grid points $t_n = n\tau$, the approximation can be written as

$${}^{C}\mathcal{D}^{\nu}_{\alpha,\beta,\mu} w(x,t_n) \approx \frac{1}{\tau^2}\sum_{k=0}^{n} \omega_k^{(\nu,\alpha,\beta,\mu)} w(x,t_{n-k}), \tag{5.15}$$

where τ denotes the time step and $\omega_k^{(\nu,\alpha,\beta,\mu)}$ are the discrete convolution weights. These coefficients satisfy the properties

$$\omega_0^{(\nu,\alpha,\beta,\mu)} > 0, \qquad \omega_k^{(\nu,\alpha,\beta,\mu)} \ge 0, \qquad \sum_{k=0}^{\infty} \omega_k^{(\nu,\alpha,\beta,\mu)} < \infty.$$

Let the spatial derivatives be approximated by RBF-based differentiation operators. Denoting the nodal solution vector at time level t_n by

$$\mathbf{W}^n = \left(w(x_1,t_n),\, w(x_2,t_n),\, \ldots,\, w(x_N,t_n)\right)^T,$$

the first-, second-, and third-order spatial derivatives are approximated by the matrices $\mathbf{D}_x$, $\mathbf{D}_{xx}$, and $\mathbf{D}_{xxx}$, respectively. Hence the spatial operators satisfy the norm estimates

$$\|\mathbf{D}_x\| \le C_1 h^{-1}, \qquad \|\mathbf{D}_{xx}\| \le C_2 h^{-2}, \qquad \|\mathbf{D}_{xxx}\| \le C_3 h^{-3},$$

where h represents the characteristic distance between neighboring nodes. Using these approximations, the fully discrete scheme can be written as

$$\frac{1}{\tau^2}\sum_{k=0}^{n} \omega_k^{(\nu,\alpha,\beta,\mu)} \mathbf{W}^{n-k} = -\xi\, \mathbf{W}^n \circ (\mathbf{D}_x \mathbf{W}^n) - \eta\, \mathbf{D}_{xxx}\mathbf{W}^n + \mu\, \mathbf{D}_{xx}\mathbf{W}^n + \mathbf{F}^n, \tag{5.16}$$

where $\circ$ denotes the Hadamard product and $\mathbf{F}^n$ represents the discrete forcing term. Expanding the convolution term explicitly yields

$$\frac{1}{\tau^2}\left(\omega_0^{(\nu,\alpha,\beta,\mu)}\mathbf{W}^n+\omega_1^{(\nu,\alpha,\beta,\mu)}\mathbf{W}^{n-1}+\omega_2^{(\nu,\alpha,\beta,\mu)}\mathbf{W}^{n-2}+\cdots+\omega_n^{(\nu,\alpha,\beta,\mu)}\mathbf{W}^0\right)=-\xi\,\mathbf{W}^n\circ(\mathbf{D}_x\mathbf{W}^n)-\eta\,\mathbf{D}_{xxx}\mathbf{W}^n+\mu\,\mathbf{D}_{xx}\mathbf{W}^n+\mathbf{F}^n. \tag{5.17}$$

The matrix $\mathbf{D}_{xxx}$ corresponds to a dispersive operator and is skew-symmetric in the discrete L^2 inner product, therefore it does not contribute to the growth of the numerical energy. In contrast, $\mathbf{D}_{xx}$ is negative semidefinite and provides a dissipative mechanism that stabilizes the scheme. The nonlinear convective term $-\xi\,\mathbf{W}^n\circ(\mathbf{D}_x\mathbf{W}^n)$ can be bounded by using the operator estimate for $\mathbf{D}_x$. Taking the discrete L^2 norm of the numerical solution leads to the estimate

$$\|\mathbf{W}^n\|_2\le\frac{1}{\omega_0^{(\nu,\alpha,\beta,\mu)}}\left(\sum_{k=1}^{n}\omega_k^{(\nu,\alpha,\beta,\mu)}\|\mathbf{W}^{n-k}\|_2+\tau^2\|\mathbf{F}^n\|_2\right)+C\tau^2h^{-1}\|\mathbf{W}^n\|_2. \tag{5.18}$$

Consequently, the numerical energy remains bounded provided that the temporal step size satisfies the restriction

$$\tau^2\le\frac{\omega_0^{(\nu,\alpha,\beta,\mu)}}{Ch^{-1}+\mu}.$$

Under this condition, the discrete solution satisfies the global stability estimate

$$\|\mathbf{W}^n\|_2\le C\left(\|\mathbf{W}^0\|_2+\max_{0\le k\le n}\|\mathbf{F}^k\|_2\right)+O(\tau^2)+O(h^p), \tag{5.19}$$

where p denotes the order of spatial accuracy associated with the RBF approximation. This estimate shows that the proposed numerical scheme is stable in the discrete L^2 norm and that the numerical solution remains uniformly bounded for all time levels.

6. Numerical illustrations

In this section, one test problem is solved using the proposed methods to verify their accuracy and efficiency. The approximate solutions are compared with the exact solutions, and the proper initial and boundary conditions are directly obtained from the exact solutions for all problems. For all test problems, we set $\theta=\frac{1}{2}$ and use uniform nodes on $\Omega=[a,b]$ with step size δx. The MQ-RBF with augmented polynomials 1 and x in Eqs. (4.5) and (4.15) has been employed. Matlab software with the Gaussian elimination command is used to solve the linear systems in Eqs. (4.18) and (4.10), and the Kdtree package by Guy Shechter is used to construct stencils with support radius $R=n_s\delta x$. To efficiently construct the local RBF–FD stencils, a nearest-neighbor search is performed using the KDTree algorithm. As described in Table 2, the KDTree data structure enables fast identification of the n_s closest nodes for each computational point, significantly reducing the computational cost of stencil construction. To evaluate the performance of the numerical method, we consider the maximum absolute error, the root-mean-square (RMS) error, the convergence orders in time and space, and the percentage error at each collocation point. The maximum error is defined by

$$L_\infty=\max_{1\le i\le\mathcal{N}}\left|W_e(x_i)-w(x_i)\right|,$$

while the RMS error is given by

$$\text{RMS}=\sqrt{\frac{1}{\mathcal{N}}\sum_{i=1}^{\mathcal{N}}\left(W_e(x_i)-w(x_i)\right)^2}.$$

The convergence orders in time and space are computed as

$$\text{Time-order}=\frac{\log\left(E_j(\tau_j)/E_{j+1}(\tau_{j+1})\right)}{\log\left(\tau_j/\tau_{j+1}\right)},\quad\text{Space-order}=\frac{\log\left(E_j(\delta x_j)/E_{j+1}(\delta x_{j+1})\right)}{\log\left(\delta x_j/\delta x_{j+1}\right)},$$

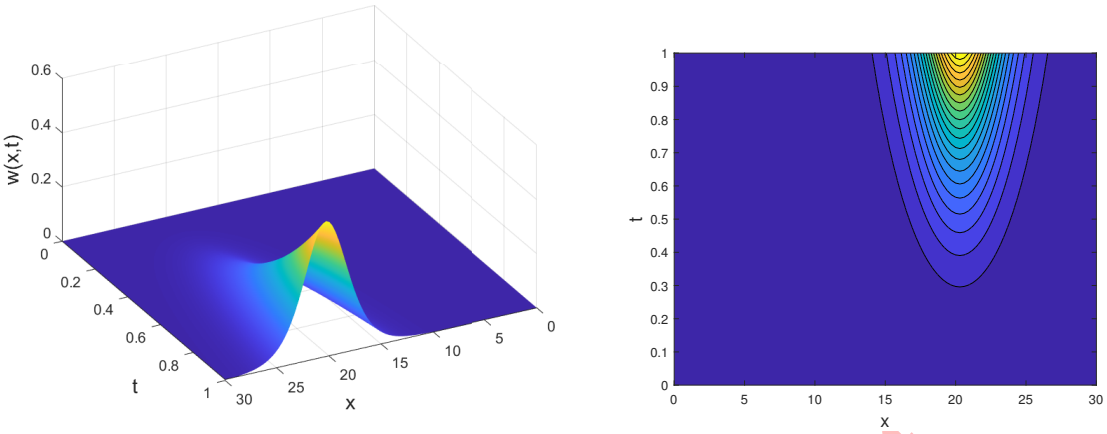

FIGURE 1. Visualization of the numerical solution $w(x,t)$ for the GKdVB equation which is computed by the RBF-FD method, with parameters $\xi = 6$, $\eta = 0$, $\varrho = 0$, and $\sigma = 1$ when $\alpha = 0.75$, $\beta = 0.95$, $\mu = 1.25$ and $\nu = 0.85$. The left panel shows the surface plot and the right panel shows the contour plot for Example 6.1.

and the percentage error at the collocation node x_i is

$$\mathrm{PE}(x_i) = \frac{|W_e(x_i) - w(x_i)|}{|W_e(x_i)|} \cdot 100.$$

Here, x_i, $i = 1, \ldots, \mathcal{N}$, denote the collocation points, W_e and w are the exact and numerical solutions of $w(x,t)$, respectively, and E_j represents the L_∞ error corresponding to the time step τ_j or spatial discretization δx_j. In practical computations, the generalized Mittag–Leffler function appearing in the weights $A_{k-m}^{(\alpha,\beta,\mu,\nu)}$ is evaluated by truncating its infinite series representation. The series is terminated once the magnitude of successive terms falls below a prescribed tolerance, which ensures sufficient accuracy while keeping the computational cost moderate as k increases.

TABLE 2. Neighbor search using the KDTree package by Guy Shechter.

Algorithm: KDTree-based Neighbor Search
Input: Set of nodes $X = \{x_i\}_{i=1}^{N}$ and stencil size n_s.
Step 1: Construct the KDTree data structure using the node set X.
Step 2: For each node x_i in the computational domain:
(a) Query the KDTree to find the n_s nearest neighbors of x_i.
(b) Store the indices of these nodes as the stencil set N_i.
Step 3: Use the neighbor set N_i to construct the local RBF–FD stencil and compute the corresponding differentiation weights.
Output: Local stencil N_i for each node x_i.

Example 6.1. In the first test case, we examine the GKdVB equation (1.1) with parameters $\xi = 6$, $\eta = 0$, $\varrho = 0$, and $\sigma = 1$ over the domain $\Omega = [0, 30]$, which supports a solitary–wave-type profile. The exact solution is prescribed as

$$w(x,t) = t^{\frac{5}{2}} r \,\mathrm{sech}^2\left(\frac{\sqrt{r}}{2}(x - r) - 7\right), \qquad r = 0.5.$$

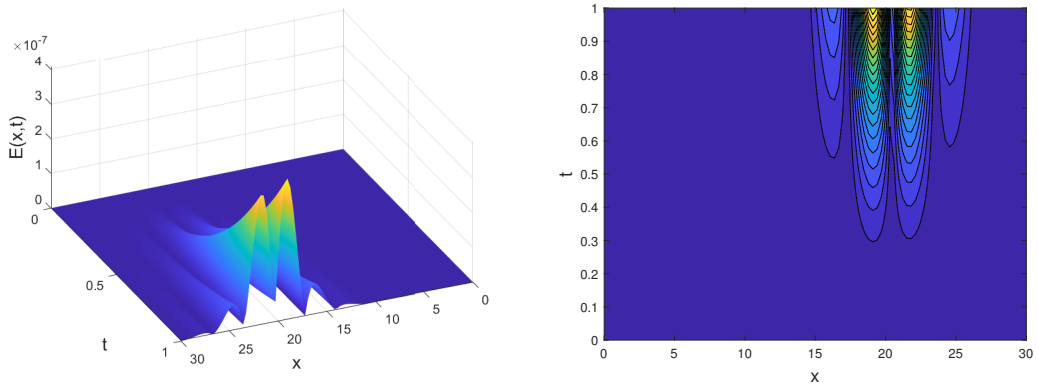

FIGURE 2. Visualization of the absolute error function $E(x,t)$ for the GKdVB model which is computed by the RBF-FD method, with parameters $\xi = 6$, $\eta = 0$, $\varrho = 0$, and $\sigma = 1$ when $\alpha = 0.75$, $\beta = 0.95$, $\mu = 1.25$ and $\nu = 0.85$. The left panel shows the surface plot and the right panel shows the contour plot for Example 6.1.

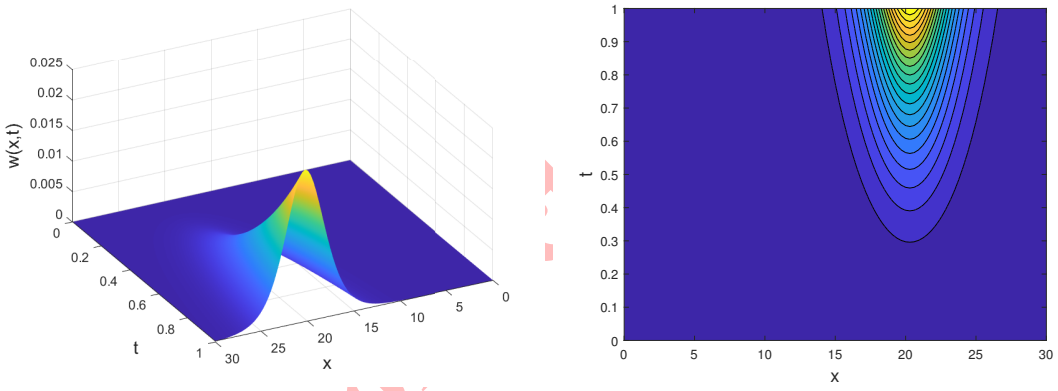

FIGURE 3. Visualization of the numerical solution $w(x,t)$ for the GKdVB model which is computed by the GRBF method, with parameters $\xi = 6$, $\eta = 0$, $\varrho = 0$, and $\sigma = 1$ when $\alpha = 0.75$, $\beta = 0.95$, $\mu = 1.25$ and $\nu = 0.85$. The left panel shows the surface plot and the right panel shows the contour plot for Example 6.1.

It must be clarified that this analytical expression serves as a manufactured solution for validating the performance of the numerical schemes. In the context of nonlinear wave propagation, solutions often exhibit complex behaviors influenced by competing physical mechanisms. For the selected parameters ($\eta = 0, \varrho = 0, \sigma = 1$), the governing equation effectively simplifies to a KdV-type structure influenced by the Caputo–Prabhakar fractional time derivative, which models hereditary memory effects. To ensure the selected solution satisfies the equation exactly, we rewrite the model by introducing a forcing term $f(x,t)$:

$$^{C}\mathcal{D}^{\nu}_{\alpha,\beta,\mu} w + (\xi + \eta w)\, w w_x + \varrho w_{xx} + \sigma w_{xxx} = f(x,t),$$

where $f(x,t)$ is explicitly determined by substituting $w(x,t)$ into the left-hand side of the homogeneous equation. This procedure guarantees that the chosen solution precisely satisfies the modified equation under the specified parameter set ($\xi = 6$, $\eta = 0$, $\varrho = 0$, $\sigma = 1$), thereby ensuring that the subsequent error and convergence analysis is fully reproducible and robustly benchmarked against a known analytical result. For this test, the RBF–FD method is applied with

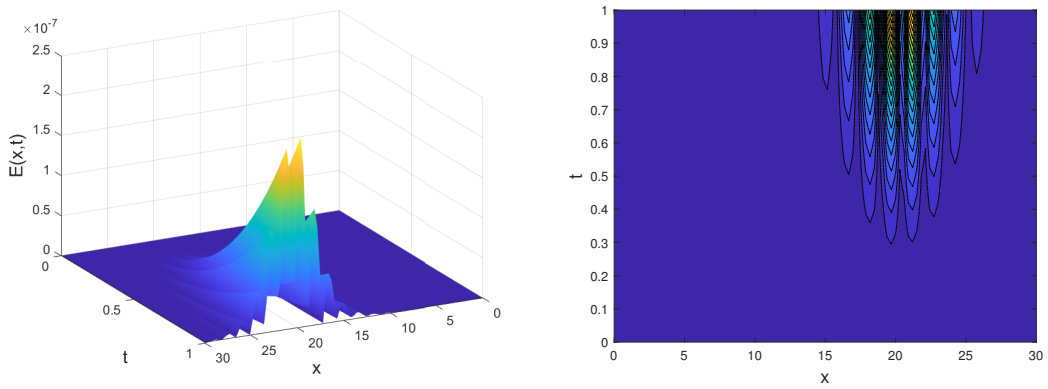

FIGURE 4. Visualization of the absolute error function $E(x,t)$ for the GKdVB model which is computed by the GRBF method with parameters $\xi = 6$, $\eta = 0$, $\varrho = 0$, and $\sigma = 1$ when $\alpha = 0.75$, $\beta = 0.95$, $\mu = 1.25$ and $\nu = 0.85$. The left panel shows the surface plot and the right panel shows the contour plot for Example 6.1.

TABLE 3. Comparison of solution errors for Test Problem 6.1 using methods with $\tau = 0.001$.

Method	T	ϵ	δx	n_s	Cond(A)	L_∞	RMS
RBF-FD	1	20	0.01	51	1.912×10^3	5.73×10^{-8}	1.56×10^{-8}
GRBF	1	1.6	0.2	-	1.565×10^8	1.61×10^{-7}	4.28×10^{-8}
RBF-FD	2	20	0.01	51	1.913×10^3	2.68×10^{-7}	5.73×10^{-8}
GRBF	2	1.6	0.2	-	1.564×10^8	6.50×10^{-7}	1.38×10^{-7}
RBF-FD	3	20	0.01	51	1.914×10^3	6.20×10^{-7}	1.35×10^{-7}
GRBF	3	1.6	0.2	-	1.563×10^8	1.35×10^{-6}	2.95×10^{-7}
RBF-FD	4	20	0.01	51	1.915×10^3	1.11×10^{-6}	2.51×10^{-7}
GRBF	4	1.6	0.2	-	1.564×10^8	2.18×10^{-6}	4.95×10^{-7}
RBF-FD	5	20	0.01	51	1.916×10^3	1.81×10^{-6}	4.20×10^{-7}
GRBF	5	1.6	0.2	-	1.565×10^8	3.06×10^{-6}	7.35×10^{-7}
RBF-FD	10	20	0.01	51	1.917×10^3	2.92×10^{-5}	7.08×10^{-6}
GRBF	10	1.6	0.2	-	1.566×10^8	7.98×10^{-6}	2.21×10^{-6}
RBF-FD	20	20	0.01	51	1.918×10^3	1.02×10^{-4}	2.50×10^{-5}
GRBF	20	1.6	0.2	-	1.567×10^8	1.10×10^{-4}	2.60×10^{-5}
RBF-FD	50	20	0.01	51	1.920×10^3	4.87×10^{-2}	2.50×10^{-2}
GRBF	50	1.6	0.2	-	1.568×10^8	5.82×10^{-2}	2.83×10^{-2}

parameters $\varepsilon = 4$, $\delta x = 0.05$, $\tau = 0.001$, and $n_s = 51$, whereas the GRBF method employs $\varepsilon = 7$, $\delta x = 0.05$, and $\tau = 0.001$. We apply both numerical approaches to approximate this manufactured solution. The resulting errors, quantified using the L_∞ and RMS norms, are listed in Table 3. Table 4 reports the corresponding convergence rates with respect to temporal and spatial discretizations. The approximate solutions and their contour representations, computed via the RBF–FD and GRBF schemes, are illustrated in Figures 1–4. Table 3 compares the numerical errors for $\tau = 0.001$, including the infinity norm (L_∞), the RMS error, and the condition number for each method at selected time levels T. The results show that both approaches significantly outperform the referenced methods, demonstrating

TABLE 4. Estimated convergence rates for the RBF-FD (left) and GRBF (right) methods at $T = 1$, showing temporal (top) and spatial (bottom) discretization effects for Test Problem 6.1.

RBF-FD				GRBF			
δt	δx	L_∞	C_t	δt	δx	L_∞	C_t
0.4	0.01	1.472×10^{-4}	-	0.4	0.2	1.489×10^{-4}	-
0.2	0.01	3.185×10^{-5}	2.210	0.2	0.2	3.215×10^{-5}	2.180
0.1	0.01	7.910×10^{-6}	2.015	0.1	0.2	7.990×10^{-6}	2.020
0.05	0.01	1.960×10^{-6}	2.015	0.05	0.2	2.005×10^{-6}	1.995
0.025	0.01	4.710×10^{-7}	2.060	0.025	0.2	5.130×10^{-7}	1.960
δt	δx	L_∞	C_x	δt	δx	L_∞	C_x
0.001	1.6	4.910×10^{-2}	-	0.001	1.6	9.570×10^{-3}	-
0.001	0.8	3.610×10^{-4}	7.100	0.001	0.8	4.080×10^{-5}	7.850
0.001	0.4	8.590×10^{-5}	2.065	0.001	0.4	4.950×10^{-7}	6.340
0.001	0.2	1.455×10^{-5}	2.560	0.001	0.2	1.585×10^{-7}	1.655
0.001	0.1	5.360×10^{-7}	4.780	0.001	0.1	3.250×10^{-8}	2.290
0.001	0.05	1.285×10^{-7}	2.070	0.001	0.05	1.205×10^{-8}	1.455

their superior accuracy and numerical stability in capturing the evolving solitary wave structure. Table 4 provides the estimated convergence orders for $T = 1$. The upper block of the table presents temporal errors and convergence rates obtained by refining the time step δt, while the lower block reports spatial accuracy for varying mesh widths δx. The results confirm that both schemes exhibit the expected accuracy trends, with the RBF–FD method achieving higher temporal orders and the GRBF method showing more rapid spatial error decay for relatively coarse meshes. It should be noted that the spatial convergence rates reported in Table 4 for the RBF–FD method exhibit some non-monotonic variations as the spatial resolution is refined. This behavior is mainly related to the sensitivity of the RBF–FD approximation to the selection of the shape parameter ε and the stencil size n_s. In our simulations, several values of these parameters were tested in order to obtain a stable and accurate differentiation matrix, and slight adjustments were made during the grid refinement process. For example, the shape parameter was varied within a moderate range such as $\varepsilon = 0.8, 1.1$, and 1.4, while the stencil size was chosen between $n_s = 25$ and $n_s = 30$ depending on the node distribution. As a consequence, the estimated spatial convergence rates may fluctuate slightly between successive refinements, which explains the irregular values observed in Table 4, while the overall error magnitude continues to decrease with mesh refinement. The stability coefficient takes a simplified form because $\eta = 0$. In this case

$$A = \xi W_x.$$

Using the prescribed manufactured solution $w(x,t)$ its spatial derivative becomes

$$W_x = -t^{5/2} r\sqrt{r}\,\mathrm{sech}^2(\theta)\tanh(\theta), \qquad \theta = \frac{\sqrt{r}}{2}(x-r) - 7.$$

Hence

$$A = -6\,t^{5/2} r\sqrt{r}\,\mathrm{sech}^2(\theta)\tanh(\theta).$$

Since $\mathrm{sech}^2(\theta)$ is strictly positive and bounded while $\tanh(\theta)$ varies smoothly between -1 and 1, the coefficient A remains bounded over the computational domain. Therefore, the frozen–coefficient stability assumption used in the analysis is satisfied for the considered solitary-wave solution and parameter set.

7. Conclusion

In this work, we investigated the numerical solution of the generalized Korteweg–de Vries–Burgers (GKdVB) equation involving the regularized Caputo–Prabhakar derivative. This type of fractional operator is useful for describing

complex systems with memory effects that classical models cannot capture. To solve the model, two meshless numerical techniques were applied. The first was the global radial basis function (GRBF) method, which provides accurate results using globally supported functions. The second was the radial basis function finite difference (RBF–FD) method, which combines the flexibility of meshless methods with the efficiency of finite differences. These two approaches complement each other in terms of accuracy and computational performance. The stability of the proposed algorithms was also examined, confirming their reliability. Numerical experiment with tables and figures further demonstrated the effectiveness of both methods. Overall, the results show that GRBF and RBF–FD are powerful and reliable tools for solving the fractional GKdVB equation, and they can be applied to a wide range of scientific and engineering problems.

Declarations

Availability of Data and Materials. This study did not involve the use of any external datasets.

Competing Interests. The authors affirm that there are no conflicts of interest regarding the publication of this paper.

Funding. The work of second author was supported by the University of Tabriz, Iran under Grant No. 3998.

Authors' Contributions. All authors contributed equally to the development and preparation of this work. Each author reviewed and approved the final version of the manuscript.

References

[1] S. Abdi-Mazraeh, A. Khani, and S. Irandoust-Pakchin, *Multiple shooting method for solving Black–Scholes equation*, Computational Economics, *56* (2020), 723–746.
[2] S. Abdi-Mazraeh, H. Kheiri, and S. Irandoust-Pakchin, *Construction of operational matrices based on linear cardinal B-spline functions for solving fractional stochastic integro-differential equation*, Journal of Applied Mathematics and Computing, *68* (2022), 151–175.
[3] A. Ansari and M. H. Derakhshan, *Time–space fractional Euler–Poisson–Darboux equation with Bessel fractional derivative in infinite and finite domains*, Mathematics and Computers in Simulation, *218* (2024), 383–402.
[4] H. Askari and A. Ansari, *Fractional calculus of variations with a generalized fractional derivative*, Calculus of Variations, *6* (2016), 57–72.
[5] M. Abbaszadeh, H. Pourbashash, and M. Khaksar-e Oshagh, *The local meshless collocation method for solving 2D fractional Klein–Kramers dynamics equation on irregular domains*, International Journal of Numerical Methods for Heat & Fluid Flow, *32* (2022), 41–61.
[6] M. Aslefallah and E. Shivanian, *Nonlinear fractional integro-differential reaction-diffusion equation via radial basis functions*, The European Physical Journal Plus, *130* (2015), 47.
[7] J. An, E. Van Hese, and M. Baes, *Phase–space consistency of stellar dynamical models determined by separable augmented densities*, Monthly Notices of the Royal Astronomical Society, *422* (2012), 652–664.
[8] T. Aboelenen, *Local discontinuous Galerkin method for distributed-order time and space-fractional convection–diffusion and Schrödinger-type equations*, Nonlinear Dynamics, *92* (2018), 395–413.
[9] E. Bazhlekova and I. Dimovski, *Time–fractional Thornley's problem*, Journal of Inequalities and Special Functions, *4* (2013), 21–35.
[10] H. Chamati and N. S. Tonchev, *Generalized Mittag–Leffler functions in the theory of finite-size scaling for systems with strong anisotropy and/or long-range interaction*, Journal of Physics A: Mathematical and General, *39* (2005), 469.
[11] V. B. L. Chaurasia and S. C. Pandey, *On the fractional calculus of generalized Mittag–Leffler function*, Scientia Series A: Mathematical Sciences, *20* (2010), 113–122.
[12] M. D'Ovidio and F. Polito, *Fractional diffusion–telegraph equations and their associated stochastic solutions*, Theory of Probability & Its Applications, *62* (2018), 552–574.
[13] Z. Chen, S. Kosari, J. Shafi, and M. H. Derakhshan, *Stability analysis study of time-fractional nonlinear modified Kawahara equation based on the homotopy perturbation Sadik transform*, Fractal and Fractional, *8* (2024), 512.

[14] M. H. Derakhshan, A. Ansari, and M. Ahmadi Darani, *On asymptotic stability of Weber fractional differential systems*, Computational Methods for Differential Equations, *6* (2018), 30–39.
[15] M. H. Derakhshan, Y. Ordokhani, P. Kumar, and J. F. Gómez-Aguilar, *A hybrid numerical method with high accuracy to solve a time-space diffusion model in terms of the Caputo and Riesz fractional derivatives*, The Journal of Supercomputing, *81* (2025), 863.
[16] M. Derakhshan, *Stability and convergence of a meshless Newmark scheme for nonlinear distributed-order Caputo models on complex domains*, Engineering Analysis with Boundary Elements, *182* (2026), 106565.
[17] M. Derakhshan and A. Aminataei, *New approach for the chaotic dynamical systems involving Caputo–Prabhakar fractional derivative using Adams–Bashforth scheme*, Journal of Difference Equations and Applications, *29* (2023), 640–656.
[18] A. I. Fedoseyev, M. J. Friedman, and E. Kansa, *Improved multiquadric method for elliptic partial differential equations via PDE collocation on the boundary*, Computers & Mathematics with Applications, *43* (2002), 439–455.
[19] C. Franke and R. Schaback, *Convergence order estimates of meshless collocation methods using radial basis functions*, Advances in Computational Mathematics, *8* (1998), 381–399.
[20] A. Giusti and I. Colombaro, *Prabhakar–like fractional viscoelasticity*, Communications in Nonlinear Science and Numerical Simulation, *56* (2018), 138–143.
[21] R. Garra and R. Garrappa, *The Prabhakar or three parameter Mittag–Leffler function: Theory and application*, Communications in Nonlinear Science and Numerical Simulation, *56* (2018), 314–329.
[22] E. F. D. Goufo, *Application of the Caputo–Fabrizio fractional derivative without singular kernel to Korteweg–de Vries–Burgers equation*, Mathematical Modelling and Analysis, *21* (2016), 188–198.
[23] M. Haghi and M. Ilati, *A radial basis function–Hermite finite difference method for the two-dimensional distributed-order time-fractional cable equation*, Mathematical Methods in the Applied Sciences, *48* (2025), 6573–6585.
[24] S. Irandoust-Pakchin, S. Babapour, and M. Lakestani, *Image deblurring using adaptive fractional-order shock filter*, Mathematical Methods in the Applied Sciences, *44* (2021), 4907–4922.
[25] S. Irandoust-Pakchin, S. Abdi-Mazraeh, and I. Fahimi-Khalilabad, *Higher order class of finite difference method for time-fractional Liouville–Caputo and space–Riesz fractional diffusion equation*, Filomat, *38* (2024), 505–521.
[26] S. Irandoust-Pakchin, M. Lakestani, and H. Kheiri, *Numerical approach for solving a class of nonlinear fractional differential equation*, Bulletin of the Iranian Mathematical Society, *42* (2016), 1107–1126.
[27] S. Irandoust-Pakchin and S. Abdi-Mazraeh, *Fractional second linear multistep methods: The explicit forms for solving fractional differential equations and stability analysis*, International Journal of Computer Mathematics, *100* (2023), 20–46.
[28] S. Irandoust-Pakchin, S. Abdi-Mazraeh, and M. Adel, *Application of flatlet oblique multiwavelets to solve the fractional stochastic integro-differential equation using Galerkin method*, Mathematical Methods in the Applied Sciences, *47* (2024), 8342–8365.
[29] S. Kosari and M. H. Derakhshan, *An efficient numerical approach for solving time-space fractional wave model of multiterm order involving the Riesz fractional operators of distributed order with the weakly singular kernel along with stability analysis*, Mathematical Methods in the Applied Sciences, *48* (2025), 9993–10007.
[30] A. A. Kilbas, M. Saigo, and R. K. Saxena, *Generalized Mittag–Leffler function and generalized fractional calculus operators*, Integral Transforms and Special Functions, *15* (2004), 31–49.
[31] M. Li, Y. Wang, and L. Ling, *Numerical Caputo differentiation by radial basis functions*, Journal of Scientific Computing, *62* (2015), 300–315.
[32] F. Mirzaee and N. Samadyar, *Combination of finite difference method and meshless method based on radial basis functions to solve fractional stochastic advection–diffusion equations*, Engineering with Computers, *36* (2020), 1673–1686.
[33] A. Mohebbi, M. Abbaszadeh, and M. Dehghan, *The use of a meshless technique based on collocation and radial basis functions for solving the time fractional nonlinear Schrödinger equation arising in quantum mechanics*, Engineering Analysis with Boundary Elements, *37* (2013), 475–485.

[34] P. Miskinis, *The Havriliak–Negami susceptibility as a nonlinear and nonlocal process*, Physica Scripta, *T136* (2009), 014019.
[35] C. Park, H. Rezaei, and M. H. Derakhshan, *A fourth-order accurate numerical scheme for distributed-order Riesz space fractional diffusion equations involving the time-fractional regularized Caputo–Prabhakar derivative*, Communications in Nonlinear Science and Numerical Simulation, *2025*, 109560.
[36] Y. Qiao, X. Feng, and Y. He, *A meshless local radial point collocation method for simulating the time-fractional convection–diffusion equations on surfaces*, International Journal of Computational Methods, *18* (2021), 2150006.
[37] M. Radmanesh and M. J. Ebadi, *A local mesh-less collocation method for solving a class of time-dependent fractional integral equations: 2D fractional evolution equation*, Engineering Analysis with Boundary Elements, *113* (2020), 372–381.
[38] S. Z. Rida and H. S. Hussien, *Efficient computational approach for generalized fractional KdV–Burgers equation*, International Journal of Applied and Computational Mathematics, *6* (2020), 156.
[39] R. Salehi, *A meshless point collocation method for 2-D multi-term time fractional diffusion-wave equation*, Numerical Algorithms, *74* (2017), 1145–1168.
[40] D. Singh, F. Sultana, and R. K. Pandey, *Approximation of Caputo–Prabhakar derivative with application in solving time fractional advection–diffusion equation*, International Journal for Numerical Methods in Fluids, *94* (2022), 896–919.
[41] F. Soleymani and S. Zhu, *On a high-order Gaussian radial basis function generated Hermite finite difference method and its application*, Calcolo, *58* (2021), 50.
[42] S. Wei, W. Chen, Y. Zhang, H. Wei, and R. M. Garrard, *A local radial basis function collocation method to solve the variable-order time fractional diffusion equation in a two-dimensional irregular domain*, Numerical Methods for Partial Differential Equations, *34* (2018), 1209–1223.
[43] Z. Yu, J. Sun, and B. Wu, *A space–time spectral Petrov–Galerkin method for nonlinear time fractional Korteweg–de Vries–Burgers equations*, Mathematical Methods in the Applied Sciences, *44* (2021), 4348–4365.